This is a preprint of an article published in the
Quarterly Journal of the Royal Meteorological Society, 135(643): 1603-1613,
DOI: 10.1002/qj.472.

The Journal is located at the following Wiley URL:
www3.interscience.wiley.com/journal/122544835/abstract

Advanced tilt correction from flow distortion effects on turbulent CO_2 fluxes in complex environments using large eddy simulation

F. Griessbaum and A. Schmidt

Institute for Landscape Ecology - Climatology, University of Münster, Münster, Germany

Published in Quarterly Journal of the Royal Meteorological Society

Abstract

Measurement of the turbulent fluxes of gases, momentum and heat can be biased by obstacles such as buildings or instrument platforms distorting the flow of air to the flux instruments. Standard methods have long been used to account for non-horizontal mean flows. Here we demonstrate a novel approach to correct for the effects of flow distortion which combines numerical flow modelling with eddy covariance measurements of the fluxes. This approach applies a flow distortion correction to the data prior to the application of the standard planar-fit and double-rotation methods. This new direction-dependent flow correction allows the determination of the correct orthogonal wind vector components and hence the vertical turbulent fluxes. We applied the method to a 10 Hz dataset of 3D wind components, temperature, and the concentrations of carbon dioxide and water vapour, as measured on top of a military tower above the city of Münster in northwest Germany during spring and summer 2007. Significant differences appeared between the fluxes that were calculated with the standard rotation methods alone and those that underwent flow distortion correction prior to the application of the rotation methods. The highest deviations of 27 % were obtained for the momentum flux. Pronounced differences of 15 % and 8 % were found for the diurnal net fluxes of carbon dioxide and water vapour, respectively. The flow distortion correction for the carbon dioxide fluxes yielded the same magnitude as the WPL (Webb-Pearman-Leuning) correction for density fluctuations.

1 Introduction

Cities act as massive anthropogenic sources of carbon dioxide. About 80 % of CO_2 emissions originate in urban areas (*Churkina*, 2008). Several studies focus on the turbulent fluxes above urban areas (e.g. *Roth*, 2000; *Grimmond et al.*, 2002; *Nemitz et al.*, 2002; *Velasco et al.*, 2005; *Vogt et al.*, 2006; *Christen et al.*, 2007; *Coutts et al.*, 2007; *Schmidt et al.*, 2008). However, the problem of flow distortion on flux measurements above or within cities needs to be addressed in more detail. Due to the heterogeneity of the urban canopy, quantification of the fluxes of CO_2, other gases, and particles above urban areas is an important scientific challenge. The need to correct the wind vector for non-horizontal mean flows in order to ensure the reliability of eddy covariance measurements is well-known (e.g. *Tanner and Thurtell*, 1969; *Hyson et al.*, 1977; *Kaimal and Finnigan*, 1994; *Wilczak et al.*, 2001; *Finnigan*, 2004). Several methods have been developed and applied to account for the deviation between the defined axes of the measured wind components and the real mean streamline coordinate system. Such deviations are induced by sonic anemometer tilt, or a slope of the surface that surrounds the measurement site. The two most common approaches to account for these deviations are the double-rotation (DR) method according to *Tanner and Thurtell* (1969) and *Hyson et al.* (1977), and the planar-fit (PF) method as introduced by *Wilczak et al.* (2001).

In addition to the simple anemometer tilt, wind measurements over complex environments are potentially affected by wind flow distortions caused by surrounding obstacles such as buildings, instrument masts, other sensors etc. This affects the horizontal flow on the one hand and additionally leads to obstacle-induced disturbance of the vertical velocity on the other. Errors in scalar fluxes as determined from the eddy covariance method can be significant if flow distortion effects are neglected (*Wyngaard*, 1988).

Flow distortion effects due to obstacles in the immediate vicinity of the anemometer location can impact the flux measurements significantly (*Wieringa*, 1980; *Dyer*, 1981, 1982; *Wyngaard*, 1982; *Mennen et al.*, 1996; *Contini et al.*, 2006). Such errors can be minimised by limiting the dataset to undistorted wind sectors and mounting the anemometers well distanced from nearby structures on a slim support. However, measurements in urban areas, on massive towers, oceanic platforms or ships are subject

to severe flow distortion effects. Various studies on flow distortion modelling were conducted on meteorological masts (*Camp and Kaufman*, 1970; *Lee et al.*, 2007; *Perrin et al.*, 2007), oceanic platforms (*Mollo-Christensen*, 1968; *Oost et al.*, 1994) and ships (*Kahma and Leppäranta*, 1981; *Yelland et al.*, 1998; *Brut et al.*, 2002; *Yelland et al.*, 2002; *Dupuis et al.*, 2003; *Weill et al.*, 2003; *Popinet et al.*, 2004; *Brut et al.*, 2005; *Moat et al.*, 2006a,b). Water flumes and wind tunnel experiments with physical platform models as well as computational fluid dynamics (CFD) modelling were used to simulate the wind field distortion.

As well as altering the speed of the wind components, in distorted airflows the wind field becomes inhomogeneous with regard to the wind direction. Since the flow distortions are sector-dependent, the azimuth of the wind also has to be taken into account when correcting the flow. With regard to measurements in complex environments with obstacle-induced flow distortions, the simple assumption of an orthogonal mean wind field becomes inappropriate. The vertical wind component, used for the calculation of the turbulent vertical exchange, may be perpendicular to the disturbed horizontal microscale wind field at the measurement point after DR or PF correction instead of giving the real vertical component of the main wind field above the fetch area.

By adulterating the regression analysis of the PF method, flow-distorted values lead to a corruption of the best-fit plane. As a consequence, an obstacle-induced flow distortion, even if it appears in only one sector, affects the PF rotated wind values from all directions and the derived turbulent fluxes, respectively. These problematic restrictions of the planar-fit method have been discussed in other studies (e.g. *Klipp et al.*, 2004; *Klipp*, 2007; *Sun*, 2007; *Richiardone et al.*, 2008).

Klipp et al. (2004) presented an approach to eliminate these effects on the calculation of the planar-fit rotation angles. The method is described as a generalised planar-fit method for measurements in areas that are disturbed by obstacles. The adjustment of the wind components follows the well-known planar-fit approach, whereas the calculation of the rotation angles is different from the multiple regression method. For this purpose the series of mean vertical wind angles, evenly spaced in wind direction, is Fourier decomposed. Since only the phase and amplitude of the fundamental Fourier frequency are directly related to the anemometer tilt, while the higher frequencies are related to obstacle-induced disturbances, this so-called Fourier Fit method derives the rotation angles from the fundamental Fourier frequency. This helps to reduce the ef-

fects of obstructions on the planar-fit adjustment. Nevertheless, this method does not correct for the effects of flow distortions, so the fluxes can only be calculated reliably for unobstructed sectors. Hence, flux values from sectors in which objects such as buildings exist still must be excluded from further analyses.

In this study we introduce an approach to account for the effects of flow distortion-induced tilt angles on the eddy covariance flux measurements. We numerically model the three-dimensional (3D) wind field around a massive radio tower (including antennas, device boxes and a crane on top of the tower) and remove the flow distortion-induced tilt angle from the dataset prior to the application of the double-rotation or planar-fit method.

It should be stressed that the results of the CFD model used within this study only comprise the changes of the mean vector wind field, which is used to adapt the tilt corrections in order to improve the eddy covariance calculations of the vertical fluxes. Hence, the approach presented includes no direct turbulence corrections, but only corrections of the mean wind field which are used to adapt the measured wind to the reference surface.

2 Methods and materials

2.1 Site description and instrumentation

The city of Münster has about 272 000 inhabitants and is located in the northwest of Germany. In contrast to its predominantly agricultural surroundings, the city of Münster itself shows similar properties to other towns concerning the massive emissions of CO_2 (*Schmidt et al.*, 2008). The measurement set-up consisted of a 3D ultrasonic anemometer YOUNG 81000V (R. M. Young Company, Traverse City, Michigan 49 686, USA) and an open path infrared CO_2 / H_2O analyser LI-COR 7500 (LICOR, Inc., Lincoln, Nebraska 68 504, USA) and a particle counter. The military tower used for the measurements is situated within the urban area of Münster, 1.8 km east of the centre of the city.

Due to the predominant southwesterly wind directions, the tower mostly lies downwind of the residential areas and the industrial sections of the city. The data of the 3D wind components, temperature, carbon dioxide, and water vapour were measured and

recorded at 10 Hz, from 30 May through to 6 September 2007. Fluxes were calculated for 30-min averaging intervals. The sensors were mounted on top of a military tower at 65 m above ground level. This height is about 40 m above the rooftops and is more than three times higher than the highest roughness elements in the surroundings of the tower (i.e. trees and city buildings). Hence, the measurements were made above the roughness sublayer (*WMO*, 2006) and were therefore not affected by flow distortion due to the surrounding city buildings.

However, some objects were mounted on the top of the tower during the measurement campaign. These included device boxes (particle counter and LI-COR control box), a small crane and several dish antennas of different sizes (Figure 1) all of which affected the wind field at the sonic anemometer position.

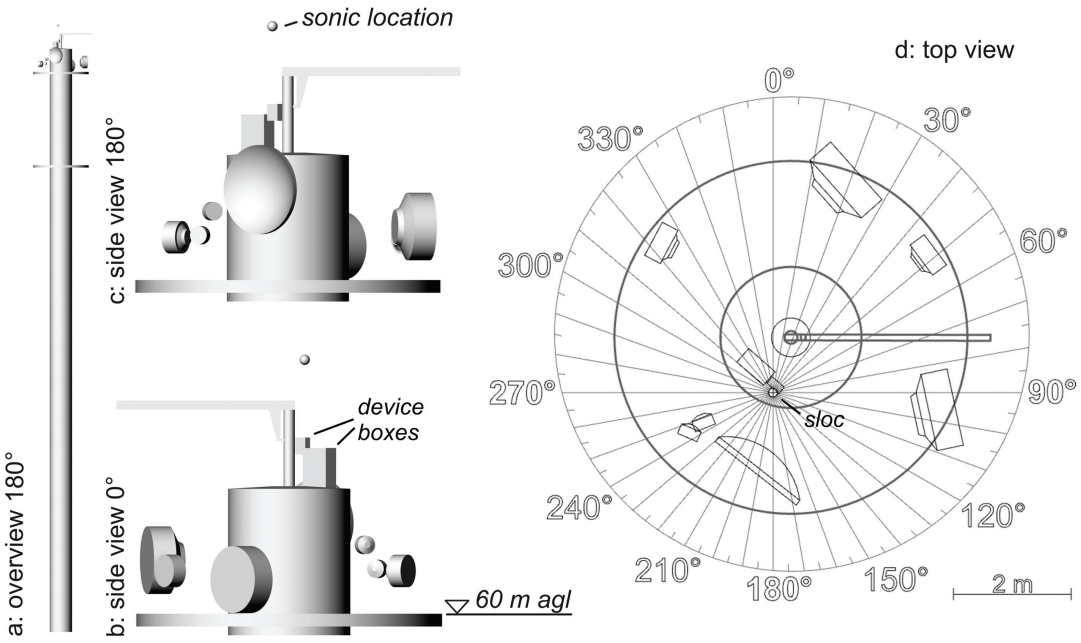

Figure 1: CAD model of military tower: (a) Overview of tower, (b) side view from North (0°) depicting the top of the tower including antennas, crane and device boxes (particle counter and LI-COR control box), (c) side view from south (180°) of tower top, (d) top view of tower indicating the locations of the antennas, crane and device boxes. The label 'sloc' indicates the sonic location. The graduated scale depicts the relative wind sectors with its centre at the sonic location.

2.2 Quality assessment of dataset

Several tests were made to ensure a high-quality dataset for further analyses and flux calculations. These included a WPL (Webb-Pearman-Leuning) correction to account for density fluctuations when calculating the fluxes of CO_2 and water vapour (*Webb et al.*, 1980) and a statistical evaluation of the steady-state conditions according to *Foken and Wichura* (1996) and *Foken* (2008).

Since the variables were measured with separate systems, a time-lag correction was conducted to synchronise the wind components and scalar variables before calculating the covariances. The corresponding time series were shifted for each sample period to find the time-step with maximum correlation (*Massman and Lee*, 2002; *Foken*, 2008).

To ensure the applicability of the eddy covariance approach, the level of mechanically induced atmospheric turbulence, as expressed by the friction velocity u_*, was obtained for each averaging interval (*Baldocchi*, 2003; *Foken et al.*, 2004). Intervals with friction velocities lower than 0.15 m s^{-1} were excluded from further analysis in order to remove cases of low turbulence (*Schmidt et al.*, 2008). Since we used a direction-dependent flow distortion correction, half-hourly sample periods with wind direction standard deviations larger than 30° were also excluded.

The LI-COR 7500 sensor head and a particle inlet were mounted close (0.15 cm) to, and northeast of, the anemometer. These objects are too small to be modelled, so data from wind directions between 350° and 55° were not used in the analysis. Due to this quality criterion just under 9 % of the whole dataset had to be removed.

2.3 Large eddy simulation

In this study, we employ the Large Eddy Simulation (LES) approach implemented in the open source (GNU General Public License, GPL) code GERRIS (*Popinet*, 2008) to model the turbulent as well as mean characteristics of the airflow around the measurement tower. The code solves the 3D time-dependent Euler equations for a velocity field,

$$U_t \; = \; -uU_x - vU_y - wU_z - \nabla p \tag{1}$$

with

$$\nabla \cdot U = 0 \tag{2}$$

and a pressure field $p = p(x, y, z, t)$ defined at location (x, y, z) and time t , for a constant density, incompressible and inviscid fluid. The adaptive mesh projection method is based on octree discretization, and a multilevel Poisson solver is used to obtain the pressure. Complex solid boundaries are represented using a Cartesian cutcell approach. The temporal discretization is based on a classical fractional-step projection method. In this study, the numerical model does not include an explicit turbulence model for turbulence scales smaller than the mesh size. Several authors (*Boris et al.*, 1992; *Porter et al.*, 1994) have shown that the numerical dissipation due to higher-order errors associated with the discrete representation of the solution describes turbulent subgrid energy transfer just as well as, or even sometimes better than, more complex LES models. The method used is described in detail in *Popinet* (2003) and was validated in a comparison of *in situ* wind measurements and numerical airflow simulations around a research vessel (*Popinet et al.*, 2004).

Previous CFD modelling of the airflow over ships has shown that the wind speed error is dependent on the relative wind direction, whereas the effect of wind speed on the wind speed error is negligible (*Yelland et al.*, 2002; *Dupuis et al.*, 2003; *Popinet et al.*, 2004). Similar results were found for CFD modelling of airflow around a land-based meteorological tower at two different wind speeds (*Perrin et al.*, 2007). Our measurement site is located well above the urban roughness sublayer. Therefore, shear is expected to be negligible and the level of turbulence as compared to the high Reynolds number around the tower's superstructure ($R \approx 10^6$) is low. Therefore, we used a constant unity inflow (not including initial turbulence nor a complex velocity profile, as e.g. a logarithmic boundary layer) imposed to the left side of the domain, simple outflow conditions to the right side, and slip conditions to the top and walls.

A 3D digital model of the tower was created from 2D drawings using the commercially available CAD (computer aided design) package Rhinoceros (*McNeel*, 2006). In order to avoid airflow reflection from the tower at the top and side boundaries, the cubical domain edge length was set to 150 m, and the 62.5 m high tower ($\varnothing$ 2.4 m, see Figure 1(a)) was placed centrally at the bottom of the domain. The detail of the solid surface is defined by the size of the mesh cells cutting the solid. This varied from 0.04 m to 0.6 m, depending on the local curvature of the tower. The adaptive mesh ap-

proach dynamically adapts to follow the evolving airflow, hence uses the finest mesh at areas of highest vorticity. In order to limit the computational cost, we chose to set the finest spatial scale to a minimum of 29 cm. Since the measurement was well above the city's roughness sublayer, a 3D model of the city was not required.

The simulation starts with a potential flow solution as initial condition: a laminar regime upstream and a turbulent regime downstream develop over time. The digital model of the military tower was rotated in the simulation domain by increments of 5° from 0° to 355° (see segments plotted in Figure 1(d)) to produce individual results for the 72 separate wind directions. Depending on the relative wind direction, 350 000 to 450 000 grid points were used to resolve the fully developed turbulence regime. The 3D wind vector (u, v, w) was recorded as a time series at a monitoring point located in the same position as the anemometer (see Figure 1(b) and (c)).

Each simulation ran for five non-dimensional timesteps $t^* = t\,U \,/\, L$, where t is the time, U is the inflow velocity and L is the domain length. A fully developed turbulence regime evolved before t^* = 1. Hence, the time window $t^* \in [1, 5]$ was used later on for calculation of mean values of 3D wind speed.

Simulated wind speeds ($g_{u,v,w}$; g indicates GERRIS flow solver) were obtained using the averaged time window. The wind speeds are then standardised by their norm U_g of the 3D wind speed at the given wind direction sector number j = 1, 2,. . . , n. The flow distortion correction factors $f_{u,v,w}$ thus obtained are then used to correct the measured wind dataset for the effects of mean flow distortion, see section 2.4.1:

$$\begin{pmatrix} f_u \\ f_v \\ f_w \end{pmatrix} = U_g^{-1} \begin{pmatrix} g_u \\ g_v \\ g_w \end{pmatrix}_j . \tag{3}$$

The resources necessary to create the digital geometry of the obstacles are small, and the computational time to numerically model the flow distortion is low. The freely available LES-code GERRIS can be operated on generic personal computers. We calculated all 72 simulations on a Linux-cluster in less than one week.

2.4 Correction methods

As a consequence of using wind fields which are affected by flow distortions, the derived vertical fluxes may strongly deviate from the real turbulent vertical exchange

between the atmosphere and the respective surface. This problem comprises measurements within the sublayer of cities in general, on platforms and towers, or measurements on ships. Furthermore, the measurement equipment itself, in particular when large instrumental boxes are used, can influence the flow in a way that the calculations of the vertical turbulent exchange are affected significantly. To account for these effects of the known obstacles, i.e. the massive tower, antennas, crane, and instrumental boxes, we used a two-step correction method:

(1) Obtaining wind direction-dependent correction factors from the LES modelling. Applying the correction factors to correct the measured dataset from flow distortion effects caused by obstacles deforming the wind field.

(2) Application of the conventional PF and DR methods on the flow-corrected dataset.

2.4.1 Enhancement of the double-rotation method

When applying the DR method, the measured wind vector components are rotated in order to force the average of the vertical wind component w_i to equal zero for each averaging interval. We further developed this method through incorporation of the wind direction-related flow distortion corrections, obtained from the LES modelling described above.

Before rotating the vector components in order to force the averages of w_i and v_i to be zero for each averaging interval of 30 minutes, the measured 10 Hz values are corrected for flow distortion using n correction vectors (for n wind directions), each containing correction factors $f_{u,v,w}$ for the three wind components. We enhanced the DR algorithm with these correction factors to account for the disturbed local wind field by a preliminary application of adopted correction vectors:

$$\begin{pmatrix} u_c \\ v_c \\ w_c \end{pmatrix} = \begin{pmatrix} u_m \\ v_m \\ w_m \end{pmatrix} - U \begin{pmatrix} f_u \\ f_v \\ f_w \end{pmatrix}_j . \tag{4}$$

The index j = 1, 2,..., n gives the number of the respective sector, i.e. the corresponding meteorological azimuth φ of the current wind vector, measured clockwise from north, and U is the norm of the current wind velocity. The wind vector components u_m, v_m and w_m are the measured values, whereas u_c, v_c, w_c are the flow

distortion-corrected wind vector components that still include the bias. The following first rotation can be expressed through:

$$\begin{pmatrix} u_1 \\ v_1 \\ w_1 \end{pmatrix} = \begin{pmatrix} \cos\phi & \sin\phi & 0 \\ -\sin\phi & \cos\phi & 0 \\ 0 & 0 & 1 \end{pmatrix} \cdot \begin{pmatrix} u_c \\ v_c \\ w_c \end{pmatrix}, \tag{5}$$

with

$$\phi = \tan^{-1}\left(\frac{\overline{v}_c}{\overline{u}_c}\right). \tag{6}$$

The second rotation, which sets $\overline{w}_i$ = 0 for each averaging interval (in our case 30 minutes), remains unchanged and is, according to *Kaimal and Finnigan* (1994), given by,

$$\begin{pmatrix} u' \\ v' \\ w' \end{pmatrix} = \begin{pmatrix} \cos\theta & 0 & \sin\theta \\ 0 & 1 & 0 \\ -\sin\theta & 0 & \cos\theta \end{pmatrix} \cdot \begin{pmatrix} u_1 \\ v_1 \\ w_1 \end{pmatrix}, \tag{7}$$

with

$$\theta = \tan^{-1}\left(\frac{\overline{w}_1}{\overline{u}_1}\right). \tag{8}$$

As the result of the step described by Equation (7), the previously corrected vertical wind component is forced to be zero for each averaging interval by also using the flow distortion-corrected horizontal wind components. Hence, we arrive at the final, flow-corrected and double-rotated wind components u', v', and w' for the calculation of the fluxes. This provides access to the corrected mean flux which is perpendicular to the source area.

Finally, the problematic, idealised, assumption of a vanishing mean vertical wind component for all halfhourly averaging intervals still remains relevant for this flow distortion-corrected double-rotation (FDR) method. Nevertheless, in contrast to the DR, the FDR yields the corrected vertical wind component, instead of just setting $\overline{w}_i$ = 0 for the disturbed wind field.

2.4.2 Enhancement of the planar-fit method

In contrast to the double-rotation method, the planar-fit method fits the wind components to an aligned plane and transforms the measured vertical wind components to be mostly perpendicular to this calculated surface (*Wilczak et al.*, 2001). The rotation angles are gained by a multiple regression analysis that respects the averaged wind vectors of the whole dataset of the respective measurement campaign. The means of the vertical wind w_i are not forced to be zero during each measurement interval of 30 minutes (for instance). Instead, after the planar-fit adjustment, $\overline{w}$ is zero when averaged over all the measurement intervals. After computation of the rotation matrix coefficients the measured wind components can be rotated to the best-fit plane by transforming the wind vector with the pitch angle α, the roll angle β, and the offset b_0. The latter also corrects the vertical wind component w. The vertical z-axis of the anemometer coordinate system is now oriented perpendicular to the mean horizontal streamlines as defined by the average wind field.
Usually, sectors that are potentially flow-distorted have to be excluded during the calculation of the planar-fit coefficients. These sectors can be identified if the surrounding region is known or, more quantitatively, by plotting the measured vertical wind component normalised by the mean wind velocity U against the azimuth angle.
For the case of a tilted anemometer within an undisturbed wind field, the curve shows a simple sinusoidal pattern. Deviations from the sinusoidal function indicate flow distortion (*Wilczak et al.*, 2001; *Klipp et al.*, 2004).

Like its archetype, the enhanced planar-fit method requires two separate steps. First, the regression coefficients and the rotation angles are calculated. In a second step, the raw 10 Hz wind components are transformed with these angles and with the respective b_0 value during the calculation of the turbulent fluxes. Thus, in order to account for the direction-dependent flow distortions, the correction factors were employed during the calculation of the rotation angles and the w-offset, as well as during the application of these corrected transformation values, to achieve a flow distortion-corrected planar-fit method, hereafter FPF method.
The application of the FPF method for the sectorrelated flow corrections is given through

$$\begin{pmatrix} u_c \\ v_c \\ w_c \end{pmatrix} = \begin{pmatrix} u_m \\ v_m \\ w_m \end{pmatrix} - U \begin{pmatrix} f_u \\ f_v \\ f_w - (b_0 \,/\, U) \end{pmatrix}_j . \tag{9}$$

In order to set $\overline{w}$ = 0 with respect to the complete dataset, all single wind data records are then transformed by application of the classical planar-fit rotation.
After that, the planar-fit adjusted wind vectors are transformed with the rotation matrix **R**

$$\begin{pmatrix} u \\ v \\ w \end{pmatrix} = \mathbf{R} \cdot \begin{pmatrix} u_c \\ v_c \\ w_c \end{pmatrix}, \tag{10}$$

with

$$\mathbf{R} = \begin{pmatrix} \cos\alpha & \sin\alpha\sin\beta & -\sin\alpha\cos\beta \\ 0 & \cos\beta & \sin\beta \\ \sin\alpha & -\sin\beta\cos\alpha & \cos\alpha\cos\beta \end{pmatrix}. \tag{11}$$

To achieve the final, flow-corrected and planar-fit adopted wind components u', v', and w', which can be used to calculate the vertical fluxes, a final, additional rotation turns the x-axis into the mean wind direction of each averaging interval i, so that $\overline{v}_i$ = 0. This step corresponds to the respective rotation given in Equation (5). Hence, after calculating the flow-corrected planar-fit coefficients that achieve the constraint given by $\overline{w}$ = 0, these adapted coefficients are applied to the measured wind values during the flux calculations in the second step. Consequently, the calculated fluxes, gained through the FPF approach, yield the true vertical fluxes of the original wind field at the tower and the applied role and pitch angles are not affected by the obstacle-induced distortions.

2.4.3 Potential and limitation of presented method

We are suggesting a method to correct flow-distorted wind fields for the flow distortion-induced tilt angle, prior to the tilt angle correction which is caused by the imperfect vertical alignment of the sonic anemometer itself.
This method is basically applicable to any environment as long as a 3D model of the

measurement platform and of the immediate vicinity of the anemometer is available for the CFD simulation. A limitation, however, lies in strongly fluctuating wakes upstream of the sonic which would increase the variance of the obtained correction factors.

Such distortion effects of obstacles upstream of the sonic location which do not only deflect the wind field, but also generate additional turbulences, can not be corrected by our approach.

In our application, the obstacle having the largest influence on the measurements was the dish antenna ($\varnothing$ = 1.8 m) in the southwest direction (see Figure 1(d)), which was located 2.2 m below the sonic anemometer. A second monitoring point, set 1.5 m below the sonic location and 0.7 m above the dish antenna, showed high standard deviations ($\sim$40 %) of the simulated vertical wind speed for southwest wind directions. This high variance indicates generation of turbulence by the antenna, besides its effect on the mean wind field. The correction factors obtained from the same wind direction show comparatively low standard deviations ($<$5 %) at the higher sonic location. Therefore, it can be assumed that the influence of the antenna at the sonic location was mostly restricted to wind field deflection.

3 Results and discussion

The distributions of the observed wind directions in Figure 2 shows that the westerly to southwesterly wind directions predominate, whereas the north and northeasterly wind directions, which were partially affected by the upwind LI-COR 7500 sensor head and aerosol inlet, are fairly rare.

The wind velocities are typically Weibull-distributed with a wind speed average of 4.4 m s^{-1} for the whole measurement campaign.

3.1 Large eddy simulation

The snapshot of a CFD simulation at 190° wind direction (Figure 3) shows a 'worst-case scenario'. The wind vector field pattern clearly displays the flow distortion caused by the tower and its superstructure. The dish antenna upstream of the sonic location causes severe vertical deflection and an updraught develops directly behind it. The

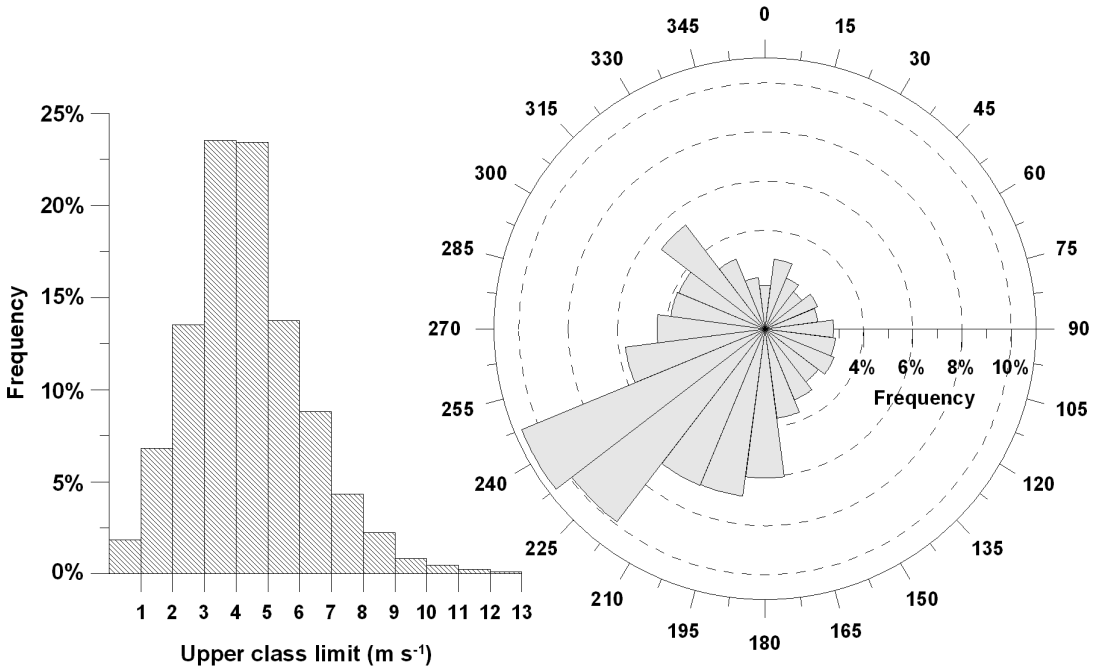

Figure 2: Percentage frequency distributions of wind direction and velocity obtained at the military tower over the complete measurement period during spring and summer 2007.

boxes below the sonic location and the crane downstream further increase the incident angle of the wind field. The resulting vertical deflection leads to a vertical displacement of the streamline passing through the sonic location. This results in a flow distortion-induced tilt angle at the sonic location. The horizontal measurement plane is, in this case, oriented upwards.

The three mean wind components u (inflow), v (lateral) and w (vertical) at the sonic location are obtained from the CFD model (see Figure 1). The wind components u and v, as defined in the CFD modelling domain, turn with the tower geometry in 5° steps, with u always being aligned with the inflow, and v being perpendicular to u.
As depicted in Figure 4, the relative wind speeds (measured speed expressed as a fraction of the undisturbed speed) indicate clearly the wind direction-dependent effect of flow distortion as caused by the obstacles at the top of the tower. All wind sectors are affected by the flow distortion, even those without any antennas or other obstacles upstream. This is the basic flow distortion caused by the massive tower's body platform. Additional wind speed errors are caused by the smaller obstacles. The highest

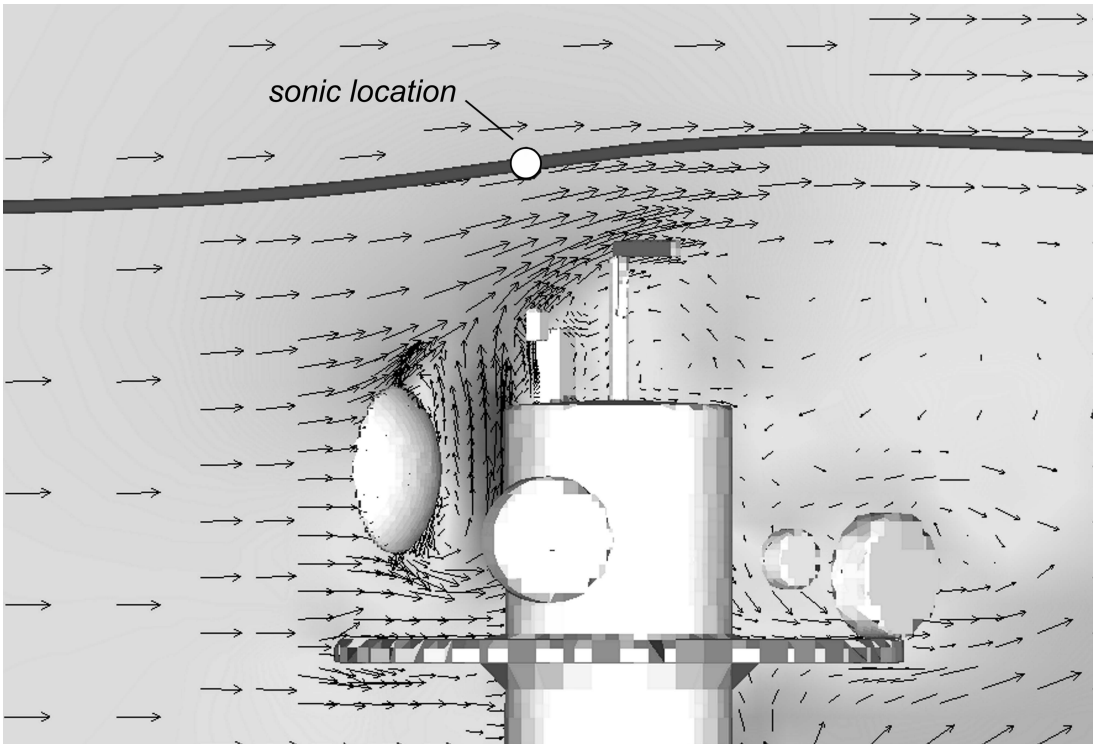

Figure 3: Flow pattern around the top of the tower at 190° relative wind direction. The velocity vector field indicates strong flow distortion due to the tower structure, antennas, device boxes and crane. The streamline passing through sonic anemometer location is elevated by the tower and its superstructure. The 190° cross-section is coloured in grey according to the vertical wind speed; dark grey indicates elevated positive wind speeds.

accelerations (up to 14 %) of vertical wind speed w are found at south-south-westerly wind directions when the biggest and uppermost dish antenna is upstream of the sonic location. The acceleration of the horizontal wind component u is decreasing from 8.5 % at 0° relative wind direction to 2 % at 180°, and increasing back to 8 % at 355°. The minimum in u for southerly winds is due to the fact that the sonic location is not at the centre of the tower, but 1 m south-southwest, meaning a longer distance of wind field contact to the tower during northerly winds with higher speed errors, and vice versa. The lateral wind component v is the least affected, except when winds are from south-southwest where the biggest dish antenna was mounted. From additional flow distortion modelling, excluding the device boxes from the CAD model, it was found that the device boxes account for 4 % of the 5 % acceleration in v.

In order to apply the correction factors from CFD modelling to the meteorological coordinate system used during measurement, with v positive to north and u positive to east, the CFD coordinate system was rotated into the meteorological one.

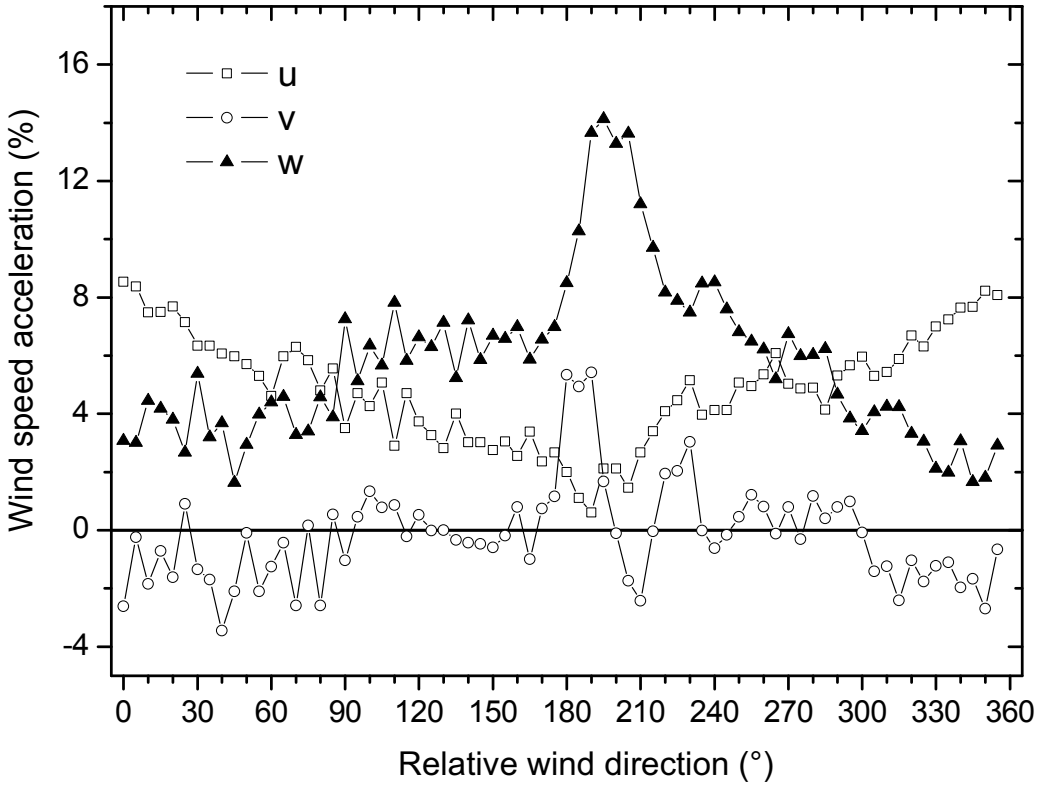

Figure 4: Modelled data at the sonic anemometer location. The ordinate indicates the relative acceleration (as a fraction of the undisturbed speed) of horizontal and vertical wind components against relative wind direction.

3.2 Enhanced planar-fit method with flow correction

In Figure 5 the measured wind velocity values before (a) and after (b) the flow correction are shown together with the calculated best-fit planes. The flow distortion clearly affects the calculated rotation angles and leads to a strongly sloped plane which is needed to achieve the criterion that $\overline{w}$ equals zero after the PF rotation. This is also supported by the relatively high offset b_0 of 0.28 m s^{-1} which is caused by the uplift of the streamlines at the cylindrical shape of the tower.

In contrast to that, the best-fit plane after flow correction in Figure 5(b) is only related to the tilt angle caused by the anemometer slope against the surface without the effects of the flow distortions. Moreover the greatly decreased b_0 value of 0.085 m s^{-1} now can be interpreted as the anemometer offset and the effect of the uplift of the wind caused by the tower's superstructure is no longer included, or at least essentially reduced.

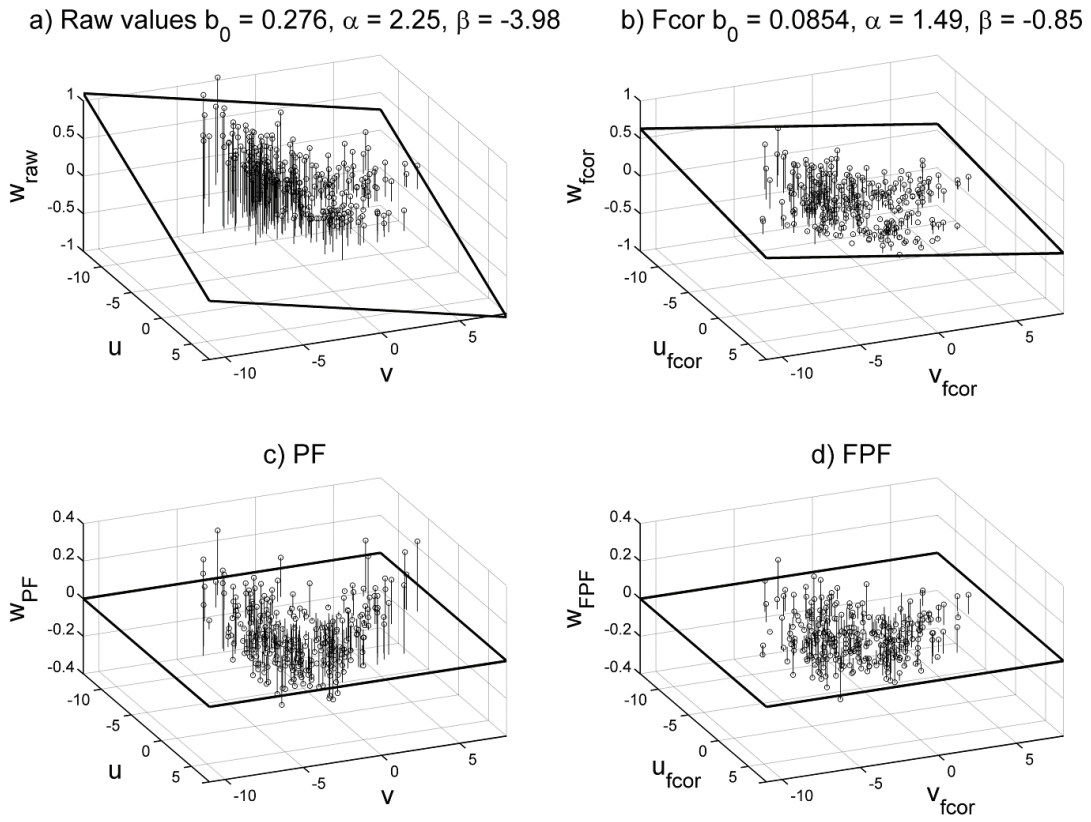

Figure 5: Mean vertical wind speeds of sonic anemometer as a function of horizontal wind speeds for (a) as measured, (b) flow distortioncorrected data, (c) after subtracting the best-fit plane from raw data, and (d) after subtracting best-fit plane from prior flow distortion-corrected data. The rectangles indicate the best-fit planes.

In Figure 6(a) the measured raw mean vertical wind velocities and the respective values after application of the flow correction (Equation 4), both plotted against wind direction, are shown. The consistent lift of the trajectories appears in the data from all wind directions (Figure 6(a)). Furthermore, the curve showing the raw values of the vertical wind velocity, w_{raw}, exhibits a large peak at the segment where the big dish

antenna was mounted (i.e. between 170° and 210°).
By contrast, the second and somewhat broader peak between 210° and 250° from north is caused by stronger winds coming from westerly directions. To exclude this phenomenon from data interpretation, the tilt angles were calculated and are shown in Figure 6(b). The tilt angles of the measured mean raw data clearly show the strong peak in the direction affected by the big dish antenna.
The uplift effect as well as the antenna-related peak could be removed from the data through the flow correction algorithm w_{fcor} as presented in Figure 6(a). Thus, due to the typical sinusoidal shape in the direction-dependent plot of the flow-corrected mean vertical wind component or the tilt angle respectively, it can be stated that the new method significantly improves the quality of the wind data by transforming the distorted flow into a corrected orthogonal wind field. These wind components can then be rotated by the DR method or PF method, in order to align the vertical component perpendicular to the surface and to calculate the turbulent vertical fluxes.

3.3 Flux comparison

Fluxes obtained with the eddy covariance method applying different correction methods (DR, FDR, PF, FPF) are displayed in Figure 7. While the buoyancy, momentum and water vapour fluxes show radiation and meteorologydriven diurnal patterns with peaks around midday, the CO_2 fluxes show pronounced emissions in the morning hours, caused by the rush-hour traffic. The CO_2 fluxes are positive through the entire day since the uptake of CO_2 by vegetation in the urban footprint is relatively small.
Comparing different methods, the PF approach yields the lowest absolute results for all parameters (Figure 7). For buoyancy, CO_2 and H_2O fluxes the DR method yields the highest fluxes, showing the same qualitative pattern in the course of a day. The momentum flux shows the largest differences between the methods. This is because the momentum flux incorporates the flow-distorted horizontal wind components (u, v) as well as the vertical wind component (w).
For an overall comparison over a one-month time period, the means of momentum and buoyancy fluxes as well as the mean diurnal net fluxes of CO_2 and water vapour are listed in Table 1 and Table 2.
Applying the PF method at the described measurement platform would result in a

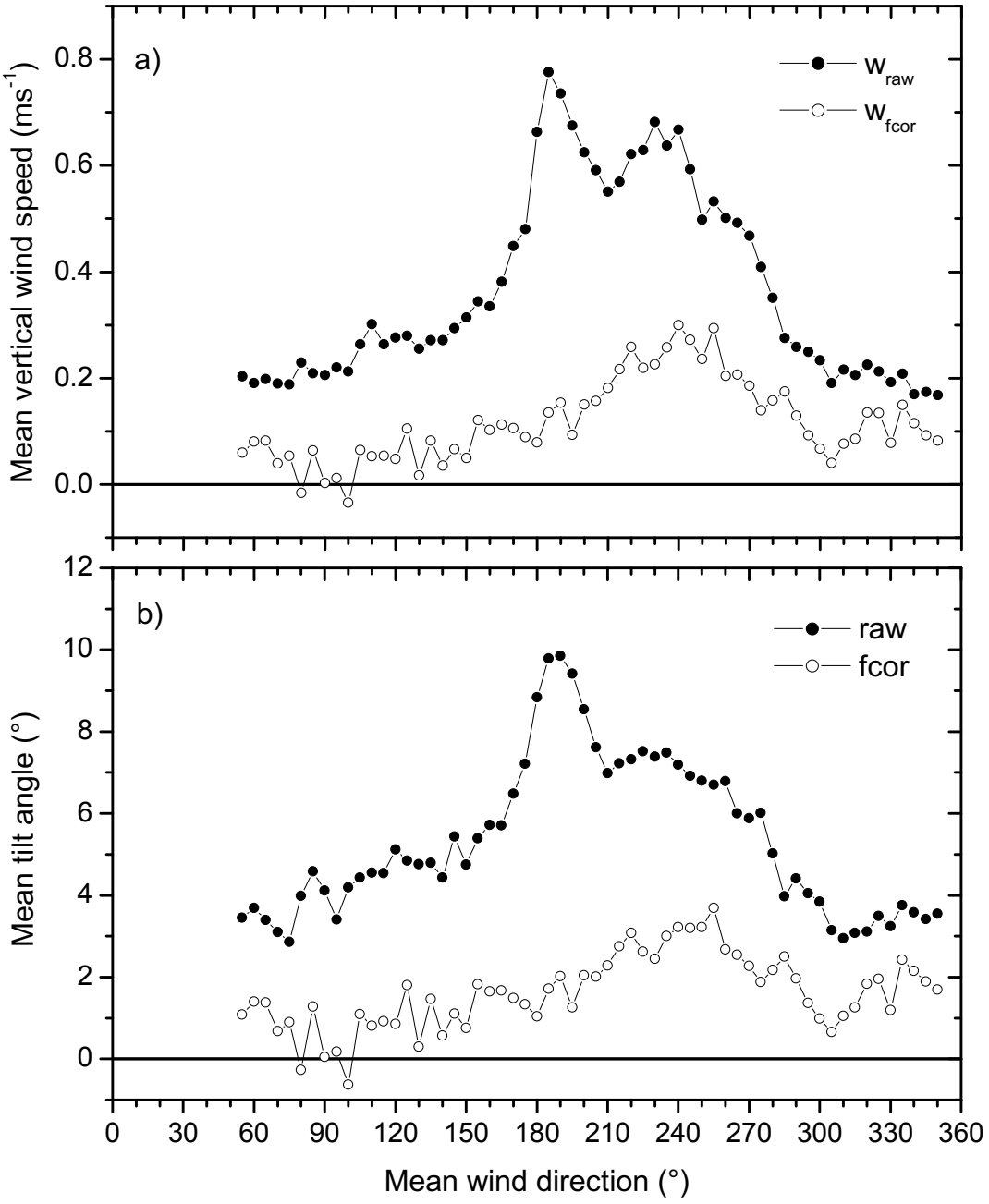

Figure 6: Mean vertical wind speed (a) and mean tilt angle (b) against mean wind direction.

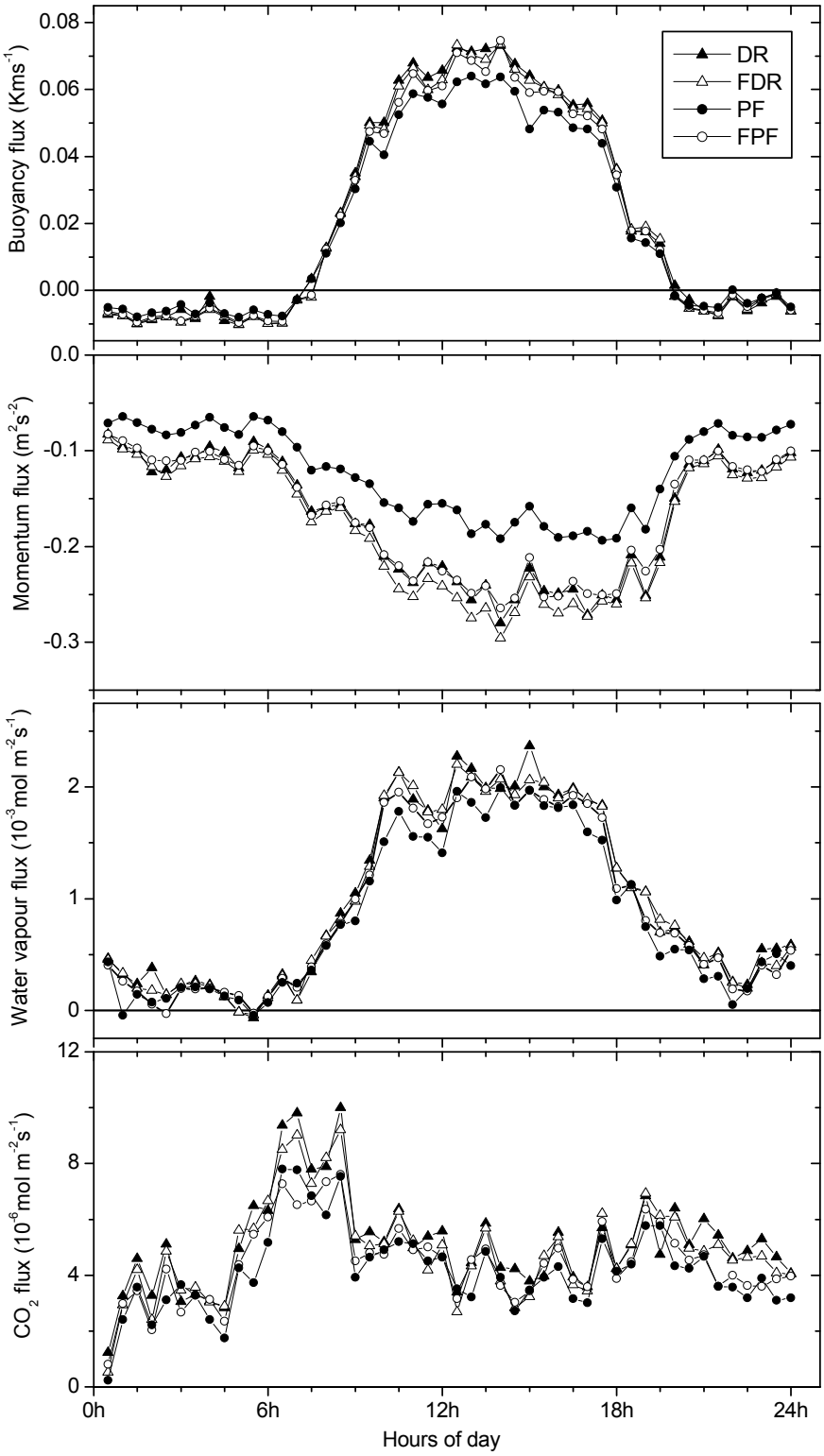

Figure 7: Mean daily fluxes of one-month dataset in August 2007 of buoyancy, momentum, water vapour and CO_2 fluxes. Each flux parameter is displayed using correction methods DR (double rotation), FDR (flow distortion-corrected double-rotation), PF (planar-fit) and FPF (flow distortion-corrected planar-fit method).

mean momentum flux underestimation of 26.6 %, compared to the FPF method (Table 1). The buoyancy fluxes show the smallest difference between the flow distortion-corrected methods FDR and FPF of 3.0 %.

The effects of flow distortion are also significant in CO_2 and water vapour fluxes. The mean diurnal net flux calculated using DR (Table 2) is 14.7 g m^{-2} d^{-1}, which overestimates the CO_2 flux by 15.4 % compared to the FPF method at 12.8 g m^{-2} d^{-1}. This is similar to the water vapour flux, yielding 1171 g m^{-2} d^{-1} using the DR method, which is 8.1 % higher than using the FPF method.

The comparison of the correction methods shows that the methods which incorporate the flow distortion correction exhibit lower fluxes than the DR method. The FPF method results in the lowest fluxes compared to the FDR method.

The flux calculations of CO_2 and water vapour comprise also the WPL-correction to account for density fluctuations. The magnitude of the WPL-correction for CO_2 fluxes is up to 20 %. Hence, for the CO_2 fluxes of this study, the magnitude of flow distortion correction is about the same as that of the WPL-correction.

Table 1: Mean fluxes for one month, August 2007.

	Momentum flux (m^2 s^{-2})				Buoyancy flux (K m s^{-1})			
Correction method	FPF	FDR	DR	PF	FPF	FDR	DR	PF
Mean flux	−0.168	−0.179	−0.17	−0.123	0.0214	0.022	0.0228	0.0198
Difference relative to FPF (%)		7.1	1.7	−26.6		3.0	6.5	−7.5

Table 2: Mean diurnal net fluxes for one month, August 2007.

	CO_2 (g m^{-2} d^{-1})				H_2O_g (g m^{-2} d^{-1})			
Correction method	FPF	FDR	DR	PF	FPF	FDR	DR	PF
Mean diurnal net flux	12.8	14.1	14.7	12.0	1083	1154	1171	989
Difference relative to FPF (%)		10.3	15.4	−6.3		6.5	8.1	-8.8

4 Summary and conclusions

In this study, we presented a novel approach to apply flow distortion modelling to tilt angle correction methods for eddy covariance flux measurements.
We numerically modelled the 3D flow distortion around a CAD geometry of a radio tower for 72 wind direction sectors, employing large eddy simulation (LES). The tower's superstructure has a strong impact on the wind field upstream of the sonic anemometer, forcing the streamline to lift vertically prior to reaching the wind sensor's location. Flow distortion correction factors ($f_{u,v,w}$) for each simulated wind direction were obtained. We enhanced two commonly applied correction methods, double rotation (DR) and planar-fit (PF), allowing corrections of flow distortion-induced tilt angle, in addition to the sonic anemometer tilt angle.
The flow distortion correction factors were applied in a two-step scheme:

(1) We corrected each 10 Hz wind speed component (u, v, w) with mean wind direction-dependent correction factors as derived from the computational fluid dynamics (CFD) modelling.

(2) We applied the common DR and PF methods on the flow distortion-corrected dataset.

The combination of steps one and two yields the flow distortion-corrected DR (FDR) and flow distortioncorrected PF (FPF) methods.
Since the method implies the constraint of vanishing sectoral vertical wind velocities without forcing the vertical wind to zero for each averaging interval, we regard the FPF method from the methodology point of view as the most appropriate tilt correction method for measurements in complex environments with unavoidable flow distortions.
The procedure of the FPF and FDR algorithms provide the ability to calculate the undisturbed mean geometry of the original wind field as it was before approaching any nearby obstructions. This enabled us to calculate the vertical fluxes that represent the respective fetch area and minimises the errors that unavoidably occur when using the disturbed microscale wind field as the reference for eddy covariance calculations. The presented method is principally applicable to any complex measurement environment. However, a limitation is given by strong turbulent wakes that are caused

by obstacles directly upstream of the sonic location. This would worsen the accuracy of the flow distortion correction factors. Furthermore, the turbulence created by such closely located obstacles can not be corrected by our approach, and would contaminate the flux measurements with respect to the source area.

The enhanced tilt correction methods, FDR and FPF, were applied to flux measurements conducted in summer 2007 over an urban area. The largest differences (PF relative to FPF) are found for the momentum flux with 26.6 %, which is due to the fact that flow distortion not only affects the vertical wind, but also the horizontal wind components which are all used in the calculation of the momentum flux. The CO_2 and H_2O fluxes exhibit significantly higher values if the commonly used DR method is used instead of the FPF method, 15.4 % and 8.1 %, respectively. Hence, the magnitude of flow distortion correction of CO_2 fluxes is in the same order as that of the WPL-correction, up to 20 %.

The flow distortion effects discussed here are only caused by the superstructure of the tower well above the city canopy. However, towers or masts that are closer or even within the urban canopy (e.g. on buildings, within street canyons) or on large platforms (e.g. ships or oceanic platforms) are subject to more severe flow distortion effects. Therefore, the expected flow distortion-induced flux errors under such conditions are potentially very large, even for the best wind sector selection. Hence measurements in such complex environments definitively need to be corrected for flow distortion.

The further development of approaches to account for the effect of complex flow distortions on flux measurements is a challenge for future studies that should combine modelling and experimental concepts. This is especially so for the development of methods which incorporate the correction of the turbulence regime itself created by nearby obstacles.

Acknowledgements

We gratefully acknowledge the Deutsche Forschungsgemeinschaft for financial support of this work (DFG, Kl623/8-1). In addition the authors would like to thank Stéphane Popinet for his support in getting started with the LES-code GERRIS, the high performance computing centres of University of Siegen and RWTH Aachen, Ger-

many, to their Linux and Windows clusters, the staff of the Manfred-von-Richthofen casern in Münster for the permission to use the military tower and their support during the installations of the measurement equipment, and M. J. Yelland for language editing of the manuscript.

References

Baldocchi, D. D. (2003), Assessing the eddy covariance technique for evaluating carbon dioxide exchange rates of ecosystems: Past, present and future, *Global Change Biol.*, *9*(4), 479–492.

Boris, J. P., F. F. Grinstein, E. S. Oran, and R. L. Kolbe (1992), New insights into large eddy simulation, *Fluid Dyn. Res.*, *10*(4-6), 199–228.

Brut, A., A. Butet, S. Planton, P. Durand, and G. Caniaux (2002), Influence of the airflow distortion on air-sea flux measurements aboard research vessel: Results of physical simulations applied to the EQUALANT99 experiment, in *15th Symposium on boundary layers and turbulence*, pp. 147–150.

Brut, A., A. Butet, P. Durand, G. Caniaux, and S. Planton (2005), Air-sea exchanges in the equatorial area from the EQUALANT99 dataset: Bulk parametrizations of turbulent fluxes corrected for airflow distortion, *Q. J. R. Meteorol. Soc.*, *131*(610), 2497–2538.

Camp, D. W., and J. W. Kaufman (1970), Comparison of tower influence on wind velocity for NASA's 150-meter meteorological tower and a wind tunnel model of tower, *J. Geophys. Res.*, *75*(6), 1117–1121.

Christen, A., E. van Gorsel, and R. Vogt (2007), Coherent structures in urban roughness sublayer turbulence, *Int. J. Climatol.*, *27*(14), 1955–1968.

Churkina, G. (2008), Modeling the carbon cycle of urban systems, *Ecol. Model.*, *216*(2), 107–113.

Contini, D., A. Donateo, and F. Belosi (2006), Accuracy of measurements of turbulent phenomena in the surface layer with an ultrasonic anemometer, *J. Atmos. Ocean. Tech.*, *23*(6), 785–801.

Coutts, A. M., J. Beringer, and N. J. Tapper (2007), Characteristics influencing the variability of urban CO_2 fluxes in Melbourne, Australia, *Atmos. Environ.*, *41*(1), 51–62.

Dupuis, H., C. Guerin, D. Hauser, A. Weill, P. Nacass, W. M. Drennan, S. Cloche, and H. C. Graber (2003), Impact of flow distortion corrections on turbulent fluxes estimated by the inertial dissipation method during the FETCH experiment on R/V L'Atalante, *J. Geophys. Res.-Oceans*, *108*(C3), Artn 8 064.

Dyer, A. J. (1981), Flow distortion by supporting structures, *Bound.-Lay. Meteorol.*, *20*(2), 243–251.

Dyer, A. J. (1982), Flow distortion by supporting structures - Reply, *Bound.-Lay. Meteorol.*, *22*(2), 267–268.

Finnigan, J. J. (2004), A re-evaluation of long-term flux measurement techniques - Part II: Coordinate systems, *Bound.-Lay. Meteorol.*, *113*(1), 1–41.

Foken, T. (2008), *Micrometeorology*, Springer, Berlin and Heidelberg.

Foken, T., and B. Wichura (1996), Tools for quality assessment of surface-based flux measurements, *Agr. Forest Meteorol.*, *78*(1-2), 83–105.

Foken, T., M. Göckede, M. Mauder, L. Mahrt, B. Amiro, and J. Munger (2004), Post-field data quality control, in *Handbook of Micrometeorology: A Guide for Surface Flux Measurement and Analysis*, edited by X. Lee, W. Massman, and B. Law, pp. 181–208, Kluwer Academic Publishers, Dordrecht.

Grimmond, C. S. B., T. S. King, F. D. Cropley, D. J. Nowak, and C. Souch (2002), Local-scale fluxes of carbon dioxide in urban environments: Methodological challenges and results from chicago, *Environ. Pollut.*, *116*, 243–254.

Hyson, P., J. R. Garratt, and R. J. Francey (1977), Algebraic and electronic corrections of measured uw covariance in lower atmosphere, *J. Appl. Meteorol.*, *16*(1), 43–47.

Kahma, K. K., and M. Leppäranta (1981), On errors in wind speed observations on R/V Aranda, *Geophysica*, *17*, 155–165.

Kaimal, J., and J. Finnigan (1994), *Atmospheric Boundary Layer Flows: Their Structure and Measurement*, Oxford University Press, New York.

Klipp, C. (2007), Wind direction dependence of atmospheric boundary layer turbulence parameters in the urban roughness sublayer, *J. Appl. Meteorol. Clim.*, *46*(12), 2086–2097.

Klipp, C., S. Chang, C. Williamson, G. Huynh, D. Garvey, and Y. Yang (2004), A generalized planar fit method for sonic anemometer tilt correction. preprints, in *16th Symposium on Boundary Layers and Turbulence*, Amer. Meteor. Soc., Portland, ME.

Lee, T., C. L. Lin, and C. A. Friehe (2007), Large-eddy simulation of air flow around a wall-mounted circular cylinder and a tripod tower, *J. Turbul.*, *8*(29), 1–28.

Massman, W. J., and X. Lee (2002), Eddy covariance flux corrections and uncertainties in long-term studies of carbon and energy exchanges, *Agr. Forest Meteorol.*, *113*(1-4), 121–144.

McNeel (2006), *Rhinoceros 4.0*.

Mennen, M. G., H. J. M. A. Zwart, J. E. M. Hogenkamp, and J. W. Erisman (1996), Flow distortion errors caused by rigid obstacles in dry deposition measurement systems, *Bound.-Lay. Meteorol.*, *81*(3-4), 353–371.

Moat, B. I., M. J. Yelland, and A. F. Molland (2006a), Quantifying the airflow distortion over merchant ships. Part II: Application of the model results, *J. Atmos. Ocean. Tech.*, *23*(3), 351–360.

Moat, B. I., M. J. Yelland, R. W. Pascal, and A. F. Molland (2006b), Quantifying the airflow distortion over merchant ships. Part I: Validation of a CFD model, *J. Atmos. Ocean. Tech.*, *23*(3), 341–350.

Mollo-Christensen, E. (1968), Wind tunnel test of the superstructure of th R/V *Flip* for assessment of wind field distortion, *Tech. rep.*, Rept. 68-2, ONR Contract NR 083-236 Fluid Dynamics Lab.

Nemitz, E., K. J. Hargreaves, A. G. McDonald, J. R. Dorsey, and D. Fowler (2002), Meteorological measurements of the urban heat budget and CO_2 emissions on a city scale, *Environ. Sci. Technol.*, *36*(14), 3139–3146.

Oost, W. A., C. W. Fairall, J. B. Edson, S. D. Smith, R. J. Anderson, J. A. B. Wills, K. B. Katsaros, and J. DeCosmo (1994), Flow distortion calculations and their application in HEXMAX, *J. Atmos. Ocean. Tech.*, *11*(2), 366–386.

Perrin, D., N. McMahon, M. Crane, H. J. Ruskin, L. Crane, and B. Hurley (2007), The effect of a meteorological tower on its top-mounted anemometer, *Appl. Energ.*, *84*(4), 413–424.

Popinet, S. (2003), Gerris: A tree-based adaptive solver for the incompressible Euler equations in complex geometries, *J. Comput. Phys.*, *190*(2), 572–600.

Popinet, S. (2008), *The Gerris Flow Solver, version 1.2.0*.

Popinet, S., M. Smith, and C. Stevens (2004), Experimental and numerical study of the turbulence characteristics of airflow around a research vessel, *J. Atmos. Ocean. Tech.*, *21*(10), 1575–1589.

Porter, D. H., A. Pouquet, and P. R. Woodward (1994), Kolmogorov-like spectra in decaying 3-dimensional supersonic flows, *Phys. Fluids*, *6*(6), 2133–2142.

Richiardone, R., E. Giampiccolo, S. Ferrarese, and M. Manfrin (2008), Detection of flow distortions and systematic errors in sonic anemometry using the planar fit method, *Bound.-Lay. Meteorol.*, *128*(2), 277–302.

Roth, M. (2000), Review of atmospheric turbulence over cities, *Q. J. R. Meteorol. Soc.*, *126*(564), 941–990.

Schmidt, A., T. Wrzesinsky, and O. Klemm (2008), Gap filling and quality assessment of CO_2 and water vapour fluxes above an urban area with radial basis function neural networks, *Bound.-Lay. Meteorol.*, *126*(3), 389–413.

Sun, J. L. (2007), Tilt corrections over complex terrain and their implication for CO_2 transport, *Bound.-Lay. Meteorol.*, *124*(2), 143–159.

Tanner, C., and G. Thurtell (1969), Anemoclinometer measurements of Reynolds stress and heat transport in the atmospheric surface layer, *ECOM 66-G22-F, ECOM, United States Army Electronics Command, Research and Developement*.

Velasco, E., S. Pressley, E. Allwine, H. Westberg, and B. Lamb (2005), Measurements of CO_2 fluxes from the mexico city urban landscape, *Atmos. Environ.*, *39*(38), 7433–7446.

Vogt, R., A. Christen, M. W. Rotach, M. Roth, and A. N. V. Satyanarayana (2006), Temporal dynamics of CO_2 fluxes and profiles over a central European city, *Theor. Appl. Climatol.*, *84*(1-3), 117–126.

Webb, E. K., G. I. Pearman, and R. Leuning (1980), Correction of flux measurements for density effects due to heat and water-vapor transfer, *Q. J. R. Meteorol. Soc.*, *106*(447), 85–100.

Weill, A., L. Eymard, G. Caniaux, D. Hauser, S. Planton, H. Dupuis, A. Brut, C. Guerin, P. Nacass, A. Butet, S. Cloche, R. Pedreros, P. Durand, D. Bourras, H. Giordani, G. Lachaud, and G. Bouhours (2003), Toward a better determination of turbulent air-sea fluxes from several experiments, *J. Climate.*, *16*(4), 600–618.

Wieringa, J. (1980), A revaluation of the Kansas mast influence on measurements of stress and cup anemometer overspeeding, *Bound.-Lay. Meteorol.*, *18*(4), 411–430.

Wilczak, J. M., S. P. Oncley, and S. A. Stage (2001), Sonic anemometer tilt correction algorithms, *Bound.-Lay. Meteorol.*, *99*(1), 127–150.

WMO (2006), *Initial guidance to obtain representative meteorological observations at urban sites. Instruments and observing methods*, Report No. 81, WMO/TD-No. 1250, Geneva, 47 pp. ed.

Wyngaard, J. C. (1982), Flow distortion by supporting structures - comments, *Bound.-Lay. Meteorol.*, *22*(2), 263–265.

Wyngaard, J. C. (1988), Flow-distortion effects on scalar flux measurements in the surface-layer - Implications for sensor design, *Bound.-Lay. Meteorol.*, *42*(1-2), 19–26.

Yelland, M. J., B. I. Moat, P. K. Taylor, R. W. Pascal, J. Hutchings, and V. C. Cornell (1998), Wind stress measurements from the open ocean corrected for airflow distortion by the ship, *J. Phys. Oceanogr.*, *28*(7), 1511–1526.

Yelland, M. J., B. I. Moat, R. W. Pascal, and D. I. Berry (2002), CFD model estimates of the airflow distortion over research ships and the impact on momentum flux measurements, *J. Atmos. Ocean. Tech.*, *19*(10), 1477–1499.